# Combined HRTEM and PEELS Analysis of Nanoporous Amorphous Carbon

by

J.L. PENG, X.D. FAN and L.A. BURSILL

School of Physics, The University of Melbourne
Parkville, 3052, Vic., Australia

Received

Both the mass density (1.37 kgm/m$^3$) and $sp^3/sp^2+sp^3$ bonding fraction (0.15) were determined for an unusual nanoporous amorphous carbon consisting of curved single graphitic sheets. A combination of high-resolution transmission electron microscopy (HRTEM) and parallel electron energy loss spectroscopy (PEELS) was used. The values of these two parameters provide important constraints for the determination of the structure of this relatively low density variety of nanoporous carbon. The results are relevant also in the search for negatively-curved Schwarzite-related carbon structures. New data are also presented for highly-oriented pyrollytic graphite (HOPG), chemically vapour deposited (CVD) diamond, $C_{60}$, glassy carbon (GC) and evaporated amorphous carbon (EAC); these are compared with the results for NAC. Kramers-Kronig analysis KKA) of the low-loss PEELS data shows that the band gaps of both NAC and EAC are collapsed relative to that of CVD diamond.

## 1. Introduction

The synthesis of diamond by chemical vapour deposition (CVD) and the discovery of fullerene $C_{60}$ and carbon nanotubes[1] offer new opportunities for the science of carbon. The range of disordered carbons is wide, covering soots, chars, carbon fibres, colloidal graphite, glassy carbon and hollow carbon spheroids. Some of these varieties may be produced using arc-discharge evaporation methods similar to those used for fullerene synthesis. There has been a parallel interest in the subject of atomic structure modelling and the prediction of the effects of atomic structure on the electronic properties.

The structure of amorphous carbon is of importance for both fundamental and applied reasons: of particular interest is the effect of disorder in a $\pi$ electron system[2]. The $\pi$ states are weakly bound and lie closer to the Fermi level than do $\sigma$ states. The filled $\pi$ states form the valence band and the empty $\pi^*$ states form the conduction band and therefore determine the size of the gap. The $\pi$-$\pi^*$ gap can vary between 0 and 5.8eV entirely as a function of medium-range correlations between $\pi$ states[2]. The absence of long-range order may have two effects, producing either a band tailing as in $\sigma$ systems, or it may allow new types of medium-range order which either enlarge or close up the gap. This dependence of the gap on medium-range order is a unique feature of $\pi$ systems[2].

In the present work, combined HRTEM and PEELS microanalysis techniques were used to analyse a nanoporous arc-discharged amorphous carbon which consists of a disordered arrangement of almost-independent graphene sheets. This material is reported as having unusual molecular sieving properties with the pore sizes of $< 5$Å, it is highly absorbent to methane and more inert to oxidation than other forms of high surface area carbons[3]. HRTEM shows this material to be highly disordered, with curved and/or puckered graphene layers. Selected area diffraction patterns retain diffuse intralayer hk0 peaks and are quite distinct from the electron diffraction patterns of typical disordered glassy carbons[4]. HRTEM also shows that the atomic structure of this material does contain some surfaces of negative curvature[4], as verified by matching HRTEM micrographs with computer simulated images obtained using the random surface schwarzite-related model of Townsend et al[5].

In this paper we present an analysis of the low-loss plasmon peaks of the PEELS spectra which yielded local densities down to about 1.3 g/cm$^{-3}$, which is lower than typical glassy carbons (about 1.5 g/cm$^{-3}$). The fraction of $sp^2/sp^2 + sp^3$ bonds was determined to be typically 0.84, by analysis of the core loss spectra; this indicates significant amounts of $\sigma$-$\pi$ mixing. The material appears to have a metallic or semimetallic nature, similar to vacuum evaporated amorphous carbon or indeed graphite. This was indicated by determining the imaginary part of the dielectric function following Kramers-Kronig analysis (KKA) of the PEELS data and comparison of the results

with corresponding results for graphite, glassy carbon and diamond.

## 2. Experimental

### (a) Specimen Preparation

Plasma-deposited carbon specimens were kindly supplied by Dr.S. Iijima (N.E.C Company, Japan); specimens for HRTEM and PEELS study were taken from the hard grey inner core of the negative carbon electrode used for d.c. arc discharge evaporation in an argon-filled vessel at 50 torr. Details of this method of preparation have been published by Ebbeson[6,7]. This material consists of a large amount of hard nanoporous amorphous carbon (NAC) (grey in colour) mixed with small squat nanotubes and hollow polyhedral nanoparticles (black and soft).

Specimen for electron microscopy were prepared by simply placing clean, dry grey carbon powder onto a 1000 mesh copper grids in order to prevent extraneous electron beam irradiation damage and contamination due to chemical contamination.

### (b) High Resolution Electron Microscopy

HRTEM was used to select areas which appeared relatively homogeneous and of slowing increasing thickness. Images were recorded using a JEOL-4000EX electron microscope operating at 400kev; the spherical aberration coefficient of the ultra-high resolution pole-pieces was Cs=0.94mm and the effective Scherzer or interpretable image resolution is 0.17nm. The specimen height was carefully adjusted to an optimum focussing current, when the objective lens astigmatism as well as the optical alignment parameters could be set precisely against calibrated values. PEELS data were rejected unless there was no apparent microstructual damage or specimen contamination over the area being illuminated by the electron beam; this was monitored by comparing images before and after recording the electron energy loss spectra.

### (c) Electron Energy-Loss Spectroscopy

A Gatan Parallel Detection Electron spectrometer (Model 666) attached to the JEOL-4000EX electron microscope was used to obtain electron energy loss spectra and the HRTEM images recorded. The resolution of the spectra was determined by measuring the full width at half-maximum (FWHM) of the zero-loss peak; this was typically close to 1.4ev when the JEOL-4000EX was operated at 100kv. All PEELS data referred to here were recorded at 100kV.

All spectra were collected at identical convergence and collection angles and were typically measured from areas of about 120nm in diameter, recording times were 120s for core loss and 0.3s for low loss. Spliced segment processing was often used to piece together a continuous spectrum from two segments of spectra acquired over low and higher energy-loss ranges.

For anisotropic crystals such as graphitic structures, the excitation probability for electronic transitions depends on the direction of the electric field in the crystal, so that the peak structure in the energy loss spectrum also depends on the direction of the scattering vector[8]. In order to eliminate orientation effects, the spectra of graphite were taken with the incident beam perpenticular to the c-axis, these results will be compared with optical refractive index measurements in the discussion below.

For comparison purposes, HRTEM images and PEELS spectra from other carbon-based materials were acquired under identical condition; some referred to in this paper include a commercial include glassy carbon (GC), CVD diamond and evaporated amorphous carbon (EAC).

### (d) PEELS Analysis Procedures

### (i) Single-Electron Scattering

All spectra were deconvoluted to obtain the single scattering distribution (SSD) using the Fourier-Log method[9]. The zero-loss peaks were removed by fitting a symmetric zero-loss peak to the negative-energy tail in each of the spectra. Both of these processes were carried out using the Gatan EL/P software (version 2.1.1).

### (ii) Calculation of Local Atomic Density

The local density of specimen was estimated by measuring the energy $E_p$ of the plasmon peak in the low loss region of PEELS spectra. The dominant peak in the loss function is the collective excitation of all valence electrons known as plasmon peak. As the energy of the plasmon is proportional to the square root of the density of the total number of valence electrons, it provides a measure of the density since each carbon atom contributes four valence electrons to the plasmons. We make use of the single free electron per atom model[8], where

$$E_p = E_g + h(N_e/4\pi\epsilon_0 m^*)^{1/2} \tag{1}$$

and $E_g$ is the band gap energy; this is zero for graphite or graphite-like material which typically behaves as a semi-metal[2] and 5-6eV for diamond; $N_e$ is the electron density, i.e. the number of free electrons/cm$^3$ which contribute to the valence band plasmon, $\epsilon_0$ is the permittivity of free space, h is Planck's constant and $m^*$ is an effective electron mass, which differs from the rest mass $m_0$ of the electrons; the latter may be expressed as

$$m^* = \chi m_0, \tag{2}$$

where $\chi$ defines a calibration constant. This is chosen so that the PEELS data for the various specimens are consistent with the values of the density, $\rho$, reported for graphite,

glassy-carbon and diamond, taken from the literature[2,8].

Consequently, the mass density of the specimen can be derived as follows:

$$\rho = 3.6 \times 10^{-3} \chi E_p^2 \tag{3}$$

where $\chi$=0.86 was calibrated by taking the density of graphite as $\rho$ =2.267g/cm$^3$ and $E_p$=27.0ev, the experimental value of the bulk plasmon energy for graphite.

### (iii) Measurement of the sp$^2$ Bonding Fraction

Quantitative information on the concentration sp$^2$ carbons was obtained by analysis of the near-edge structure of the core loss spectra; thus the 1s to $\pi^*$ edge gives direct evidence on the existence or non-existence of sp$^2$ bonded carbons[8,9]. The calculation of the fraction of sp$^2$ bonded carbon atoms in carbon-like materials is made by comparing the contribution of the 1s to $\pi^*$ peak in the carbon k-edge spectra to that of graphite. Integration of the counts in the $\pi^*$ peak from the rising edge to the peak maximum gives values which are proportional to the number of $\pi$ bonded electrons in the material. Graphitized carbon has 100% sp$^2$ bonds. This is taken as the reference material, so that the fraction of sp$^2$ bonded atoms can be determined by the determining the ratio of the $\pi^*$ peak integral for an unknown material over that for highly oriented graphitized carbon[9]. Then, the fraction of sp$^2$ bonds present (f) is calculated using

$$f = I_{u\pi^*} I_g(\Delta E) / I_{g\pi^*} I_u(\Delta E) exp((t_u - t_g)/\lambda) \tag{4}$$

where $I_{g\pi^*}$ and $I_{u\pi^*}$ are the integrals from the leading edge to the 1s to $\pi^*$ peak of the graphitized and unknown carbons respectively. The factor exp(t/$\lambda$) is applied to correct for multiple scattering which tends to reduce the intensity of the $\pi^*$ peak. $I_g(\Delta E)$ and $I_u(\Delta E)$ are the integrals over some energy window, $\Delta E$, of the graphitized and unknown carbons and are included to normalise the k-edges collected from the different specimens.

In practice, f can be derived from $f = f_u/f_g$, where $f_u$ and $f_g$ are the fractions of $sp^2/sp^2 + sp^3$ bonds calculated by extracting the $sp^2$ content from the relative area of the $\pi^*$ edge and the leading edge of the $\sigma^*$ step in the core loss region PEELS for the unknown carbon and graphite respectively.

### (iv) Kramers-Kronig Analysis

Kramers-Kronig analysis (KKA) enables the energy dependence of the real part ($\epsilon_1$) and the imaginary part ($\epsilon_2$) of the permittivity to be calculated from the energy loss function, which is performed according to the method of Johnson[8-11]. There exits the possibility of obtaining additional information which may be helpful in measuring the band gap and detecting the presence of interband transitions.

First, the single scattering loss function is obtained as above. The dielectric function is then calculated for the low-loss region of the PEELS using a sinusoidal Fourier transform and an inverse cosinusoidal Fourier transform[11]. This method has the great advantage of being fast in comparison with "traditional" numerical methods and it does not involve the Cauchy principal pole calculation. The KKA analysis was written in C using the Macintosh Programming Workshop (MPW). It is thus inserted as a Custom Function in the GATAN EL/P program[11].

## 3. Results

### (a) HRTEM

The results from Nanoporous Amorphous Carbon (NAC) are compared with those for Evaporated Amorphous Carbon (EAC) and Glassy Carbon (GC) in Fig.1. A typical high resolution electron micrograph of NAC (Fig. 1(a)) shows the material to be a highly disordered carbon which consists of almost-independent graphene sheets. Near the edge of the specimen, the images show an overlapping tangle of single graphene sheets. Black lines in this image represent parts of the sheets which lie approximately parallel to the incident electron beam[4]. The pore size of this material has been estimated[3,4] as about 5 Å. The images are very different from those of GC, which consists of cross-linked ribbon-like multi-layer graphitic sheets with micro-pores up to a few hundred Å(Fig.1(b)). The EAC was fully disordered in three dimensions (Fig.1(c)), being quite distinct from both the NAC and GC specimens.

Selected area diffraction patterns retain diffuse interlayer (hk0) peaks for NAC (inset in Fig.1(a)), which are again quite distinct from the diffuse outer rings typical of EAC (inset in Fig. 1(c)) and the diffuse inter-layer (00l) and intra-layer (hk0) peaks of GC (inset in Fig. 1(b)).

### (b) PEELS

In the low loss region the spectra of NAC show a peak near 5.4ev originating from collective excitation of $\pi$ electrons, i.e., a $\pi$ plasmon similar to graphite and a dominant peak at 21.6ev which is the collective excitation of all electrons of $\pi+\sigma$ plasmon shifted to lower energy relative to graphite (27.0ev)[2,8,12]. The local density obtained from the $\pi + \sigma$ plasmon peak positions (Fig. 2(a)) is about 1.37 g/cm$^{-3}$, which is lower than the density of typical GC (about 1.7 g/cm$^{-3}$) and EAC (2.0 g/cm$^{-3}$). The plasmon peak positions, the local densities and the $sp^2$ bonding fractions of various types of carbon-like materials are listed in Table 1. It is worth noting that the bulk density estimated from Eq.(1) is actually an upper bound since no signal will be obtained from regions containing voids larger than a characteristic plasmon wavelength of about 5 $\mathring{A}$[13]. This effect is expected to have only marginal effects for NAC, where the void size is about 0.5nm, but it does introduce some variability for the densities obtained for

GC, where the void size ranges up to 10nm.

The near edge fine structure of the core loss regions show $sp^2$ type bonding in NAC, evident by the existence of a 1s to $\pi^*$ peak. This fine structure reflects the density of the $\pi^*$ and $\sigma^*$ unoccupied states; note the transition at 287ev into the $\pi^*$ states and at 294ev into the $\sigma^*$ states respectively. The fraction of $sp^2/sp^2 + sp^3$ bonds was calculated by extracting the $sp^2$ content from the relative areas of the $\pi^*$ edge and the leading edge of the $\sigma^*$ step in the core loss region of the PEELS (Fig.2(b)), by using the spectrum of graphite as a standard for normalisation (assuming 100% sp2 bonds). This was typically 0.84 for NAC, which showed slightly higher $\sigma$-$\pi$ mixing than did EAC (approx. 0.89, see Table 1). The fraction of $sp^2/sp^2 + sp^3$ bonds of $C_{60}$ is also included in Table 1. It has about $7 - 8\%$ $sp^3$ bonds in the structure[15].

**(c) Kramers-Kronig Analysis**

Fig.3 shows the loss function, the real part ($\epsilon_1$) and the imaginary part ($\epsilon_2$) of the dielectric function of the carbon based materials (a) CVD diamond, (b) HOPG graphite ($\bar{E} \perp$ c), (c) EAC and (d) NAC respectively. The dielectric function was obtained by KKA of the loss function.

For HOPG, there is a clear separation of the two peaks due to $\pi$ -$\pi^*$ transitions at 4.0ev and the $\sigma$ to $\sigma^*$ transition at 12 ev in the imaginary part ($\epsilon_2$) of the dielectric function (Fig.3(b)). The $\pi$ -$\pi^*$ oscillator causes a first zero crossing of $\epsilon_1$ near 6.8ev, where $\epsilon_2$ is small and the loss function

$$Im(-1/\epsilon) = \epsilon_2/{\epsilon_1}^2 + {\epsilon_2}^2 \tag{5}$$

rises to a maximum, due to the $\pi$ plasmon. The second zero crossing around 12.3ev corresponds to the $\sigma$ to $\sigma^*$ transition in $\epsilon_2$, and the third zero crossing at 27ev, where $\epsilon_2$ is again small, leads to a maximum in the loss function, i.e. the $\pi + \sigma$ plasmon peak. The singularity at E=0 is as expected for a metal or semi-metal (the band gap has closed up) which was not possible to show entirely in our spectrum due to the low energy resolution (typical 1.4ev at 100kev) and overlap of the zero loss with the $\pi$ plasmon peak typical of graphitic carbons.

For CVD diamond the interband transition between the highest occupied and the lowest unoccupied electronic states appears to have onset at about 6.0eV (see Fig.3(a)). There is also a $\sigma$ to $\sigma^*$ transition at 13.0eV in $\epsilon_2$, corresponding to a zero crossing of $\epsilon_1$. This is just the result expected for such an insulator having an energy gap of 5.8eV. There appears to be an additional interband transition at 23.4eV in $\epsilon_2$. The role of this transition in the band scheme is not understood at present[8]. However, the loss function experiment and the associated KKA analysis above does confirm that it is intrinsic to diamond. Again, $\epsilon_1$ is zero above 30eV and $\epsilon_2$ is decreasing towards zero, corresponding to a maximum of the $\sigma$ volume plasmon peak in the loss function. The

absence of a $\pi$ plasmon peak is typical of PEELS analysis of diamond.

The low loss spectra of EAC and NAC (Fig.2(a)) both have a $\pi$ plasmon at about 5eV, which was more pronounced for NAC than for EAC. The $\sigma$ to $\sigma^*$ interband transition is also found in $\epsilon_2$ for both of these spectra, i.e. at 10.2eV for EAC and 12.0eV for NAC; however, the interband transition $\pi$ -$\pi^*$ was absent (c.f. the 4eV peak for $\epsilon_2$ for HOPG, Fig.3(b)). Note that the first zero crossing occurs for $\epsilon_1 = 6.8$eV for HOPG, at 4.8eV for EAC and $< 2.5$eV for NAC.

The above results certainly confirm our expectation that the band gap of disordered and amorphous carbons in $\pi$-bonded systems is controlled by the $\pi$ states. This was deduced by comparing the imaginary part ($\epsilon_2$) of the dielectric functions for EAC and NAC with that for HOPG. Note particular the similarities of NAC and EAC. These states lie close to the Fermi level, the band gap tends to depend mainly on the medium range order. At present our PEELS resolution of 1.4eV makes it impossible to obtain reliable KKA analyses for energy loss values $<$ say 2.5eV. Thus all detail in the results (Fig.3) for $< 2.5$eV is not significant. However, given that HOPG is well known to be semimetallic, it seems fair to conclude that the band gaps for NAC and EAC are also virtually zero, certainly $< 2.5$eV.

## 4. Discussion

### (a) Characterisation of $\pi - \sigma$ mixing

Carbon atoms can adopt three different bonding configurations, $sp^3$, $sp^2$, and $sp^1$. Diamond consists of 100% $sp^3$ sites with 4-fold coordination, all four valence electrons of carbon are assigned to tetrahedrally directed $sp^3$ hybrid orbitals forming strong $\sigma$ bonds with neighbouring atoms, with bond length 1.54Åand bond angle of 109°28′. The isotropy of the bonding gives diamond its high strength and low conductivity. The density is 3.52 g/cm$^3$ (see Table 1).

By way of comparison graphite consists of hexagonal layers (six membered rings, i.e. 6MR) of 100% $sp^2$ sites with 3-fold coordination, with three of the four electrons per carbon atom assigned to trigonally directed sp2 hybrids forming strong $\sigma$ bonds within the basal plane. These layers are weakly bonded together by van der Waals forces into a ABAB stacking sequence along the c axis; the fourth electron lies in $p_z$ ($\pi$) orbitals, which are normal to the $\sigma$ bonded plane. The $\pi$ orbital forms weaker $\pi$ bonds to adjacent $\pi$ orbitals. The local ordering has bond length 1.42Å, bond angle of 120°. Conductivity and strength are high along the basal plane but low along the c axis. The electrical conductivity is classified as semimetallic and the density is 2.26 g/cm$^3$.

Studies of the electronic structure of the fullerenes[14] showed carbon allotropes of intermediate hybridization; thus a $C_{60}$ molecule exhibits an intermediate hybridization of s- and p-states lying between graphite and diamond, because the curved $C_{60}$ cluster

consists of twenty hexagons (6MR) and twelve pentagons (5MR), the form exhibiting the $sp^2$ hybridization and the later $sp^3$, two different bond length; 1.39Åedge shared by two hexagons with bond angle 120°, 1.44Å for the edge shared by a hexagon and a pentagon with bond angle of 108°, which is close to the angle of 109° 28' characteristic of ideal $sp^3$ hybridization.

In a theoretical calculation[14], the average $\pi$-orbital axial vector $\sigma$-bond hybridization for $C_{60}$ was estimated as $sp^{2.287}$ and the $\pi$-orbital fractional character was 0.085 if the hybrid orbital is locally orthogonal to the $\sigma$ and 0.081 if the hybrid orbital makes equal angles with the $\sigma$ orbitals. This prediction may be compared with $^{1}3C$ NMR results which give an estimate of only 0.03 for the fractional rehybridization in natural $C^{60}$ and with our PEELS results, which gave approximately 8% $sp^3$ bonds (see Table 1). Despite the differences in these figures, the bonding in carbon $sp^2$ carbon networks (5RM in the case of $C_{60}$) certainly contains a component of $\pi$ - $\sigma$ mixing (say 3-8%).

For EAC the PEELS result was 16% $sp^3$ (see Table 1) because there are tetrahedral bonding constraints imposed on the carbon network during growth; in addition, the $sp^2$ hybrid has a lower energy configuration than the $sp^3$. An amorphous form of diamond, i.e., disordered tetrahedral carbon (100 % $sp^3$ bonds), has been grown by a filtered vacuum arc method[15].

However, our results show that $\pi$- $\sigma$ mixing does not occcur to an extent greater than 15% for NAC. HRTEM images of NAC show that this material is highly disordered, with very little obvious graphitisation, the thread-like microstructure of curved single graphitic layers are evident. The distortion of a graphite layer by puckering, tangling or cross-linking of $sp^2$ layers, presumeably introduces various types of $sp^3$ bonded defects in the $sp^2$ graphitic network, which creates some adjacent 5- and 7- ring configurations. Near the edge of the specimen, the micrographs are consistent with a large proportion of the pore sizes lying in the nanoporous region (i.e. less than say a few Å with a narrow pore size distribution). It appears that $sp^3$ defects associated with these curved graphitic sheets may contribute to the observed $\pi$ - $\sigma$ mixing for NAC.

### (b) The NAC structure

The NAC structure is different from that of GC which has a strong system of cross-linking uniting multilayer crystallites of graphite. This tends to randomize the orientation distribution of the crystallites in a rigid, finely porous mass (see e.g. the HRTEM image in Fig.1(c)). Growth of such crystallites is strongly impeded, both by the strong cross-linking between neighbouring crystallites and by their random orientation. This indicates that there are important variations of electron density within the solid, the dimensions of the homogeneous regions being of the order of some tens of Å. However, the fine porous structure of GC does not require a significant fraction of $sp^3$ defects because no curved graphite sheets are involved. This appears to

be confirmed by the observed stability of CG under electron beam heating compared with NAC, which shows a highly disordered microstructure under intense electron irradiation which more readily transforms into quasi-spherical concentric nanoparticles (nano-onions) of diameter ca. 60Å$^3$.

In order to compare our experimental results from NAC with theoretical predictions, we show in Table 2 a list of mass densities and $sp^2$ bonding fractions for some amorphous carbons and negative curved schwarzite models[17]. Among the numerous ways of modelling amorphous carbons, a continuous random network model (CRN) was built by Beeman et al[16] which may contain a varying fraction of $sp^2$ and $sp^3$ sites by considering a bond stretching and a bond bending force for $sp^3$ sites and a four body out of plane force for $sp^2$ sites. The structure varies its average bond lengths and bond angles by topological rearrangements with no broken (dangling) bonds allowed. The density and $sp^2$ fraction (except C356) of all the Beeman models, except for C356, are considerably higher than observed for NAC. However, it is not difficult to construct irregular packings of positively-curved, fullerene-related spheroids, ellipsoids, tubes, cones or polyhedra which have the required density.

The negatively-curved graphitic sheet model of Townsend[6] (C-1248) was constructed based on a random schwarzite model of amorphous graphitic carbon. Ordinary graphite surfaces, with all six-membered rings (MR), have zero Gaussian curvature. Fullerene and related nanotube structures have positive Gaussian curvature, containing 5MR. Negatively-curved models are obtained by introducing seven and/or eight MR. The amorphous graphitic model of Townsend contains five, six, seven and eight MR, forming a network of 2D sheets with no broken bonds and therefore has both positive and negative Gaussian curvature; the model fcc, a=42.92 Åand contains 1284 C atoms. Analysis of C-1284 model[17] shows it has 380 5MR, 2998 6MR, 365 7MR and only 1 8MR. Note that this model was built in a random surface basis with virtually pure $sp^2$ bonding. The open 3D structure has topological genus 12, it consist of hexagonal graphene planes containing many ring-defects and it contains voids or open compartments. Remarkably, it is a low density amorphous carbon model which should also contain some $sp^3$ bonds although the proportion of non-6MR in C-1248 is less than that of $C_{60}$. Thus, although it has approximately the same density as we obtained for NAC, it does not immediately explain the relatively high $sp^3/sp^2+ sp^3$ ratio we obtained for NAC (i.e. 0.15).

The electronic and transport properties of the C-1248 Townsend model were studied by first-principles within the local-density approximation[17]; it was shown that such random systems with two-dimensional interaction in a three-dimensional structure is expected to be a high-resistivity metal. This is consistent with our deduction that the band gap of NAC has collapsed relative to that of diamond.

In addition to the HRTEM and electron diffraction results given above other results

have been reported in the literature[3,4] which pointed out the possibile relevance of C-1248 as a model for NAC structures. We have produced evidence that NAC and C-1248 may be very similar in density and band structure. Now remains the question whether NAC has negatively or positively curved structure? Suppose NAC has the topology of a periodic minimal surface containing saddle-shapes; these were found in the HRTEM images, due to their characteristic "elbow-shaped" contrast[4], despite the well-known overlap problem for non-projecting aperiodic structures[18]. In addition we expect some 7MR to be introduced due to $sp^3$ defects introduced by twin-like operations introduced into the graphite sheets. However, neither of these contributions would seem sufficient to achieve a total of 15% $sp^3$ bonding, implying some contributions from essentially hard diamond-like amorphous carbon. Certainly the latter possibility is quite consistent with some fine detail in the HRTEM images (Fig.1(a)). It is remarkable that NAC and EAC both contain 15% $sp^3$ bonding, although the HRTEM images are quite distinct. However, the methods of preparation are not fundamentally different.

In future work we plan to use the key results for the density and $sp^3$ bonding contribution of NAC, together with a quantitative analysis of the HRTEM images, in order to arrive at a realistic atomic structural model for this material.

**Acknowledgements**

This work was supported financially by the Australian Research Council. We are grateful for the support of Dr. A.E.C. Spargo and David Dryden with the HRTEM and PEELS facitities.

## REFERENCES


1. H.W.Kroto, J.R.Henth, S.C.O'Brien, R.F.Curl and R.E.Smalley, *Nature (Lond.)*, **318**, 162-166 (1989).
2. J.Robertson, *Prog. Solid St. Chem.*, **21**, 199-333 (1991).
3. Shik Chi Tsang, P.J.F. Harris, J. B. Claridge and M.L.H. Green, *J.Chem. Soc., Commun.*, pp. 1519-1522, (1993).
4. L.A. Bursill and L.N. Bourgeois, *Int. J. Mod. Phys. Lett. B*, **9**, 1461-1470 (1995).
5. S.J. Townsend, T.J.Lenosky, D.A. Muller, C.S.Nichols and V. Elser, *Phys.Rev.Letter.*, **69**, 921-924 (1992).
6. T.W. Ebbesen and P.J. Ajayan, *Nature (Lond.)*, **358**, 220-222 (1992).
7. T.W. Ebbesen, *Ann. Rev. Mater. Sci.*, **24**, 235-264 (1994).
8. J.Fink, *Advances in Electronic & Electron Physics*, **75**, 121-231 (1989).
9. R.F.Egerton, *Electron Energy Loss Spectroscopy in the Electron Microscope*, New York, p241 (1986).
10. D. W. Johnson, *J. Phys. A:Maths and Gen.,*, **8**, 490-495 (1975).
11. X.D.Fan, J.L.Peng and L.A. Bursill, *submitted*, (1996).
12. S.D.Berger and D.R.McKenzie, *Phil. Mag. Lett.,*, **57**, 285-290 (1988).
13. P.E. Batson and R.D. Leapman, *Proc.49th Ann. Meet. Elect. Micros. Soc. America, San Jose,*Claitors: Baton Rouge, p.474 (1991).
14. R.C.Haddon, *Phil.Trans.Roy.Soc.Lond.A*, **343**, 53-62 (1993).
15. D.R. McKenzie, D. Muller, and B.A. Pailthorpe, *Phys.Rev.Lett.*, **67**, 773-776 (1991).
16. D. Beeman, J. Silverman, R. Lynds and M.R. Anderson, *Phys.Rev.B*, **30**, 870-873 (1984).
17. M.Z. Huang and W.Y.Ching, *Phys.Rev.B*, **49**, 4987-4993 (1994).
18. L.A. Bursill, L.G. Mallison, S.R. Elliot and J.M. Thomas, *J. Phys. Chem.,*, **85**, 3604-3609 (1981).

## Figure Captions

**Figure 1**
HRTEM images showing graphitic sheet arrangements (black line contrast) for (a) nanoporous amorphous carbon (NAC); (b) evaporated amorphous carbon (EAC) and (c) glassy carbon (GC).

**Figure 2**
(a) Low-loss plasmon range PEELS for NAC.
(b) Core-loss region PEELS for NAC.

**Figure 3**
Real ($\epsilon_1$) and imaginary ($\epsilon_2$) parts of the permittivity of (a) CVD diamond; (b) HOPG; (c) EAC and (d) NAC, obtained by KKA analysis of the corresponding low-loss PEELS.

Table.1 Peak positions (eV), local density and bonding fraction of carbon-like materials, deduced by PEELS analysis

| Material | $\pi \rightarrow \pi^*$ Peak | Plasmon Peak | | $1s \rightarrow \pi^*$ Edge | $1s \rightarrow \sigma^*$ Edge | Density ($g/cm^{-3}$) | | $sp^2/sp^2+sp^3$ bonding f |
|---|---|---|---|---|---|---|---|---|
| | | $E_p$ | $(\Delta E_p)_{1/2}$ | | | $\rho$ | $\rho_0$ | |
| CVD | - | 34.1 | 31.0 | - | 294.2 | 3.51 | 3.52 | 0 % |
| HOPG | 6.4 E⊥C | 27.4 | 27.0 | 287.2 | 294.0 | 2.35 | 2.27 | 100 % |
| GC | 5.8-6.2 | 24.0 | 22.0-26.0 | 287.2 | 293.5 | 1.8 | 1.5-2.1 | 100 % |
| $C_{60}$ | 5.2-6.0 | 25.6 | 25.0 | 287.2 | 293.8 | 1.78 | 1.71 | 92 % |
| EAC | 5.0 | 23.6 | 23.0 | 285.0 | 292.9 | 2.07 | 1.99 | 86 % |
| NAC | 5.4-6.0 | 21.0 | 20.5 (C1248)* | 287.4 | 293.2 | 1.37 | 1.26 (C1248) | 84 % |

Table.2 Mass density and bonding fraction of amorphous carbon for Beeman and Schwarzite models

| Model | Density $\rho$ (g/cm$^{-3}$) | $sp^2/sp^2+sp^3$ f (%) |
|---|---|---|
| Beeman | | |
| C1120 | 2.11 | 100 |
| C340 | 2.69 | 90.9 |
| C356 | 3.21 | 48.6 |
| C519 | 3.39 | 0 |
| Random Schwarzite | | |
| C-1248 (Townsend) (Fig.2, ref.5) | 1.26 | 380-5MR, 2998-6MR, 365-7MR and 1-8MR |
| Periodic Schwarzite | | |
| P216 (Fig.1(a), ref.5) | 1.11 | |
| D216(Fig.1(b), ref.5) | 1.16 | |
| G216 | 1.18 | |
| P216(ref.5) | 1.02 | |
| P192(ref.5) | 1.16 | |
| D216(ref.5) | 1.15 | |
| D168(ref.5) | 1.28 | |
| NPAC | 1.37 | 84 |
| $C_{60}$ | 1.78 | 92 20-MR, 12-5MR |
| HOPG | 2.35 | 100 All 6-MR |
| CVD | 3.51 | 0 |

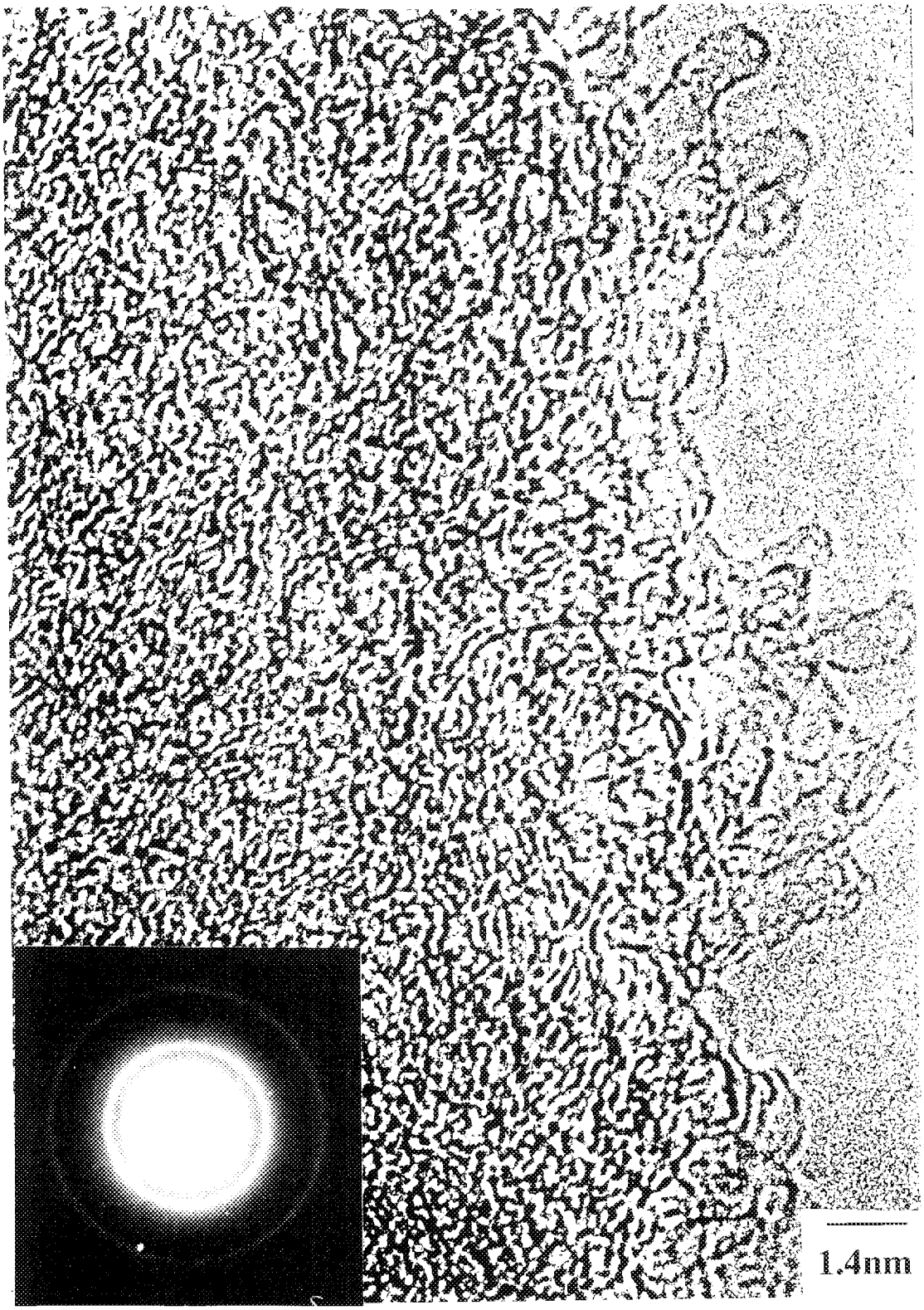


(a)

FIG. 1

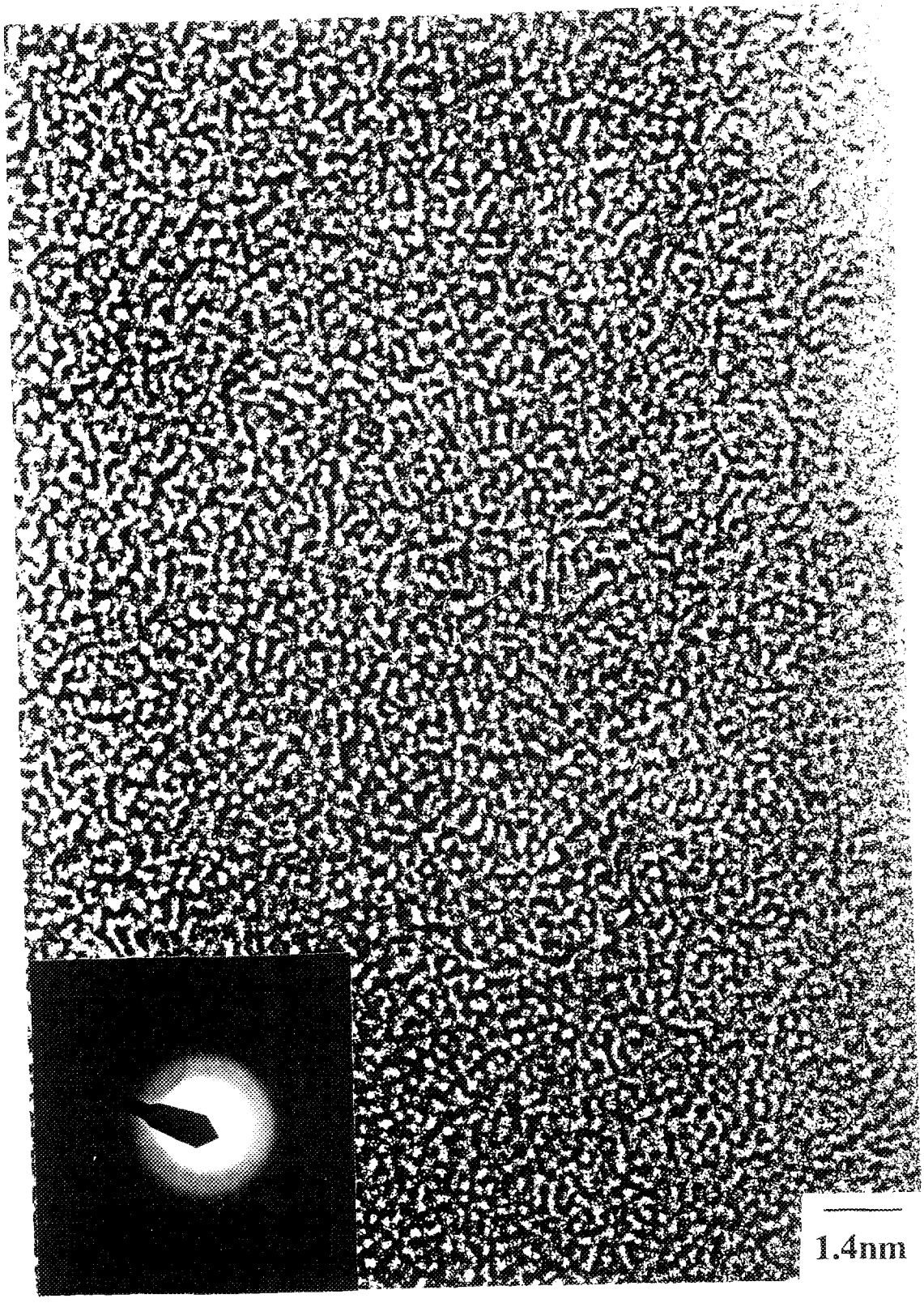


(b)

FIG. 1

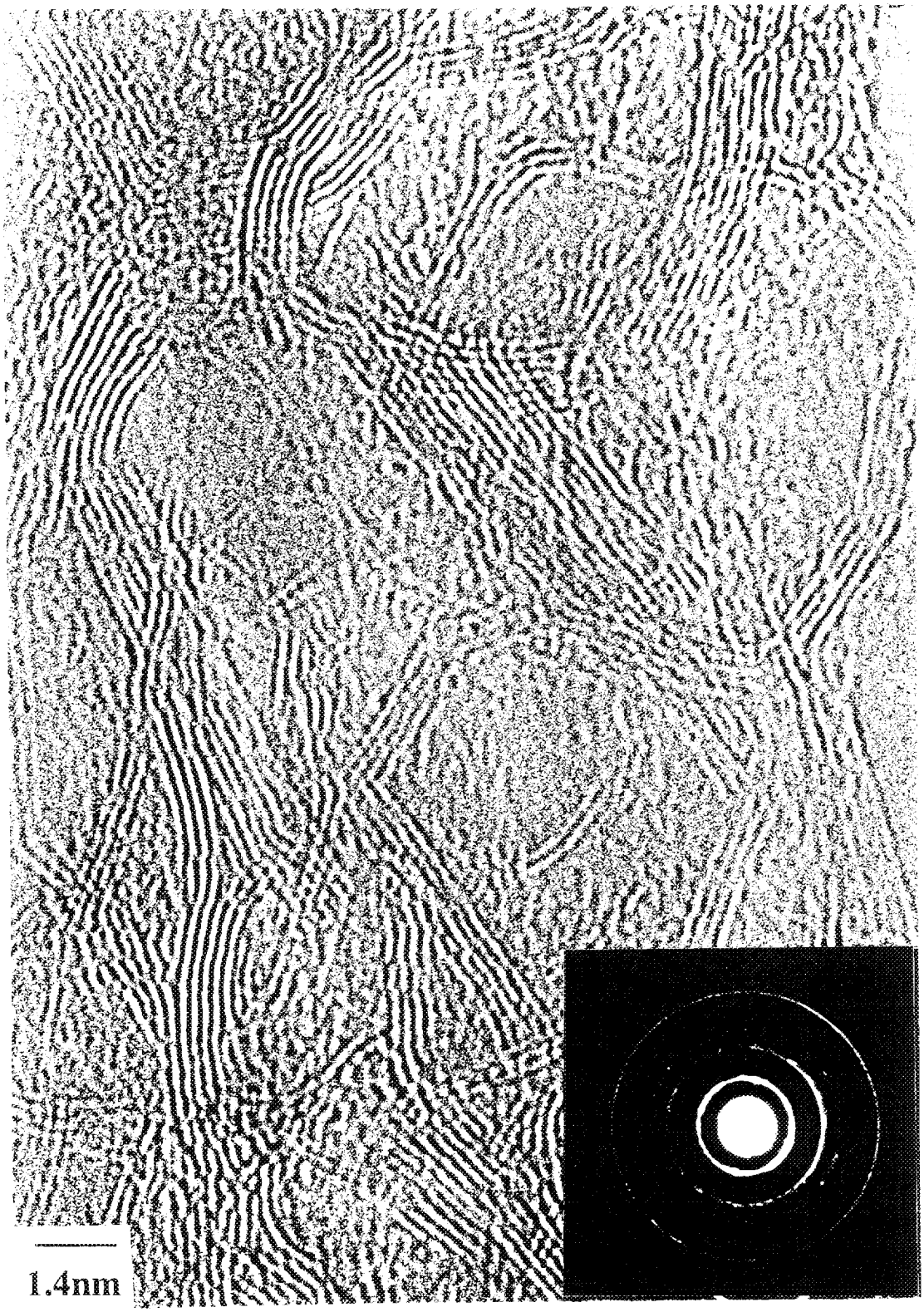


(c)

FIG. 1

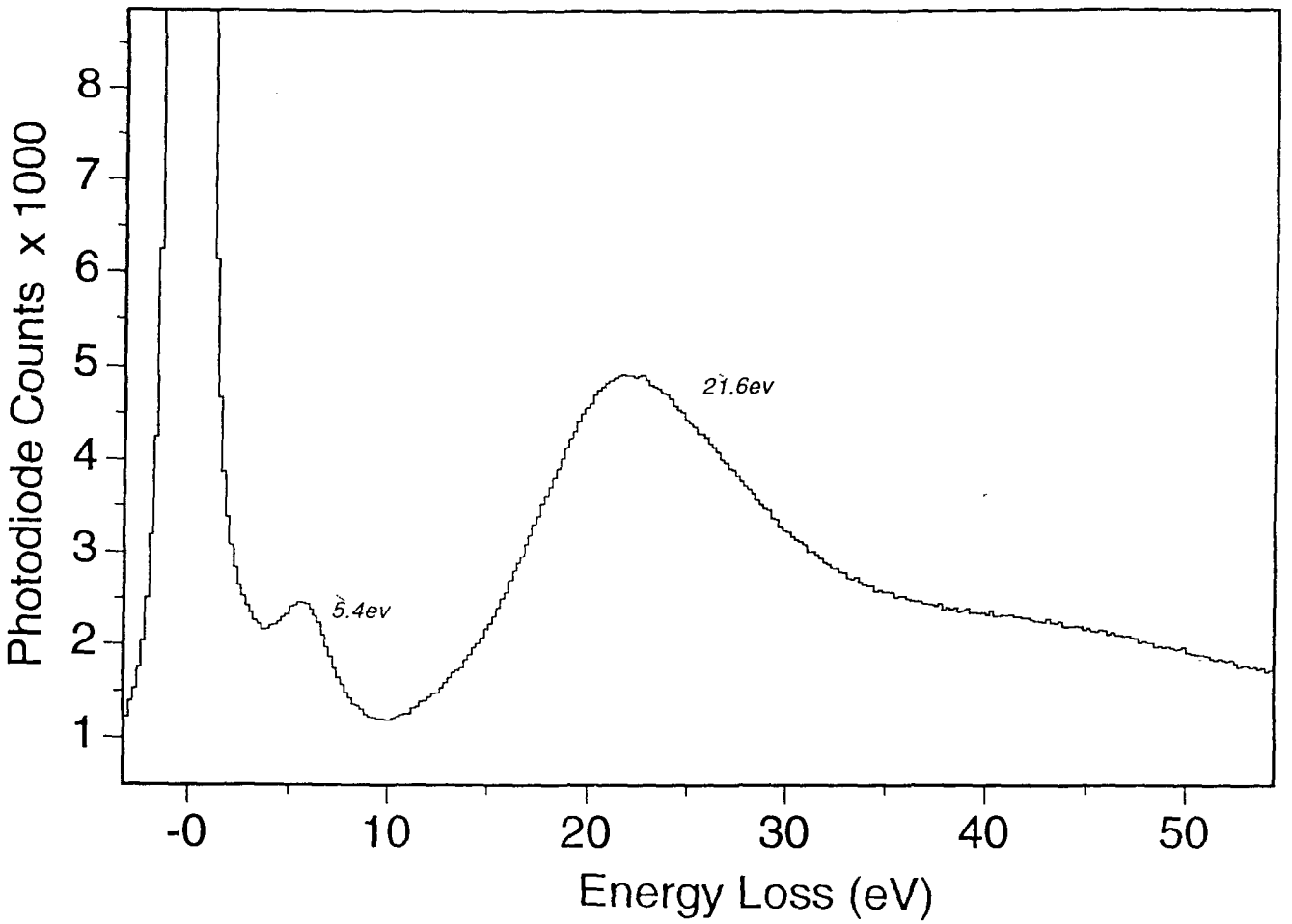
Photodiode Counts x 1000
8
7
6
5
4
3
2
1
21.6ev
5.4ev
-0
10
20
30
40
50
Energy Loss (eV)

(a)

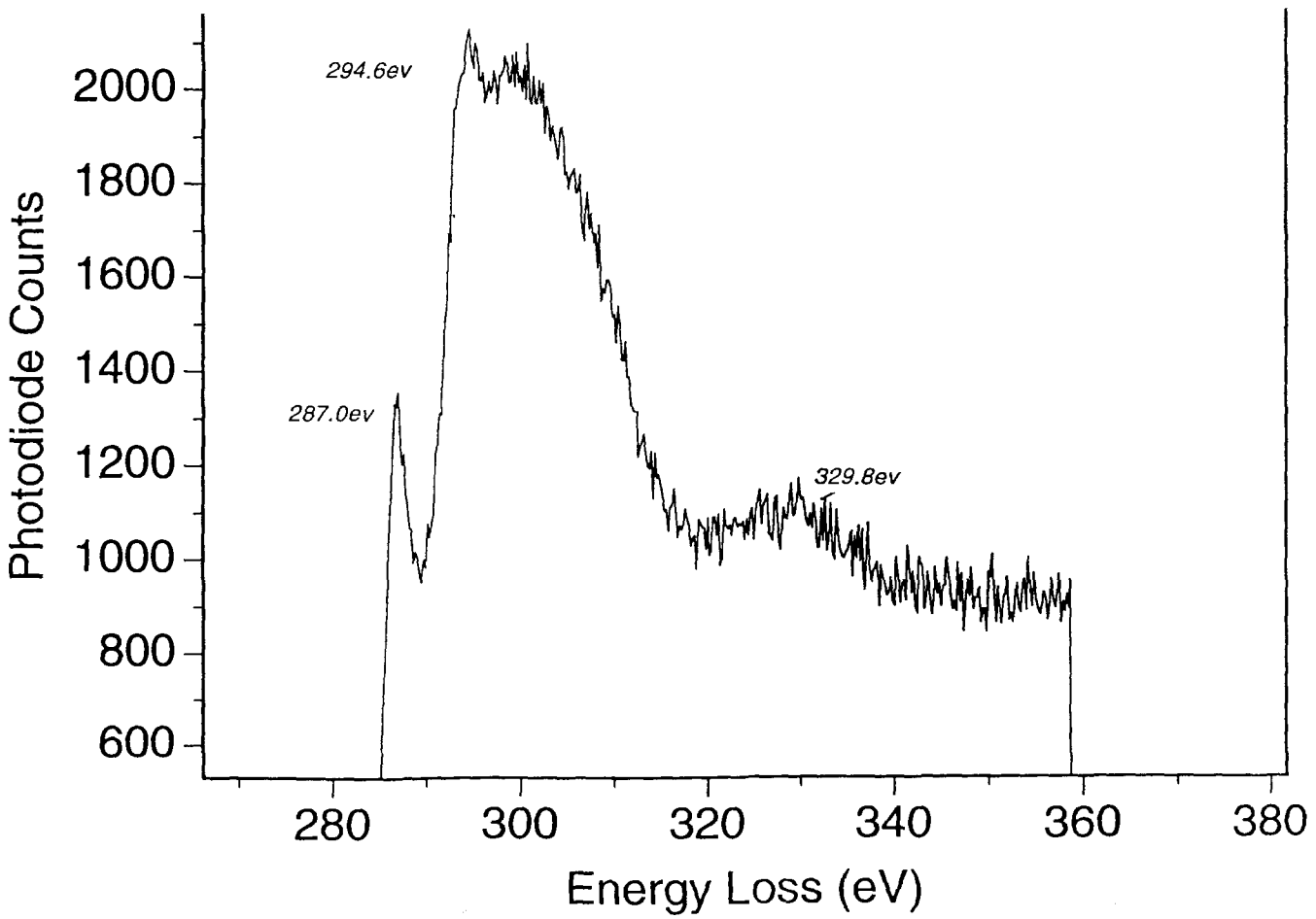
Photodiode Counts
2000
1800
1600
1400
1200
1000
800
600
294.6ev
287.0ev
329.8ev
280
300
320
340
360
380
Energy Loss (eV)

(b)

**FIG. 2**

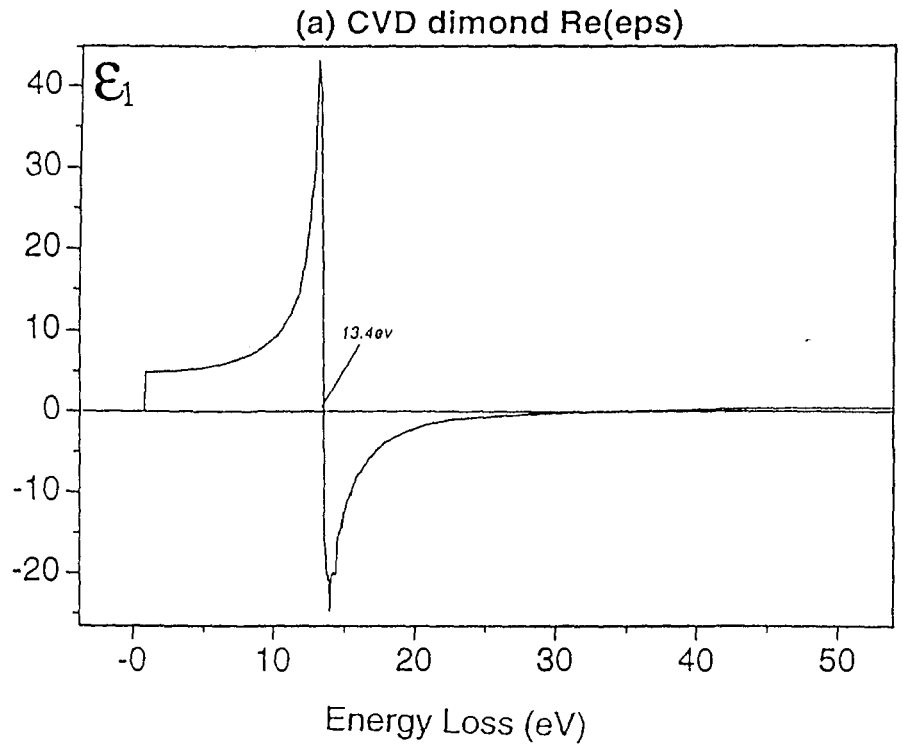
(a) CVD dimond Re(eps)
ε1
40
30
20
10
0
-10
-20
13.4ev
-0
10
20
30
40
50
Energy Loss (eV)

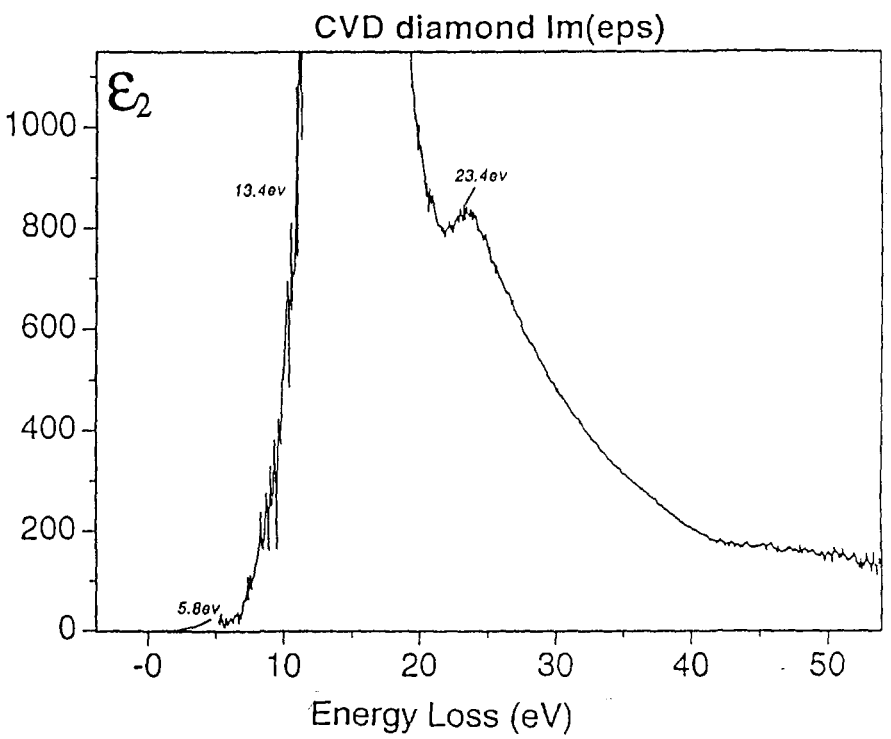
CVD diamond Im(eps)
ε2
1000
800
600
400
200
0
13.4ev
23.4ev
5.8ev
-0
10
20
30
40
50
Energy Loss (eV)

(a)

**FIG. 3**

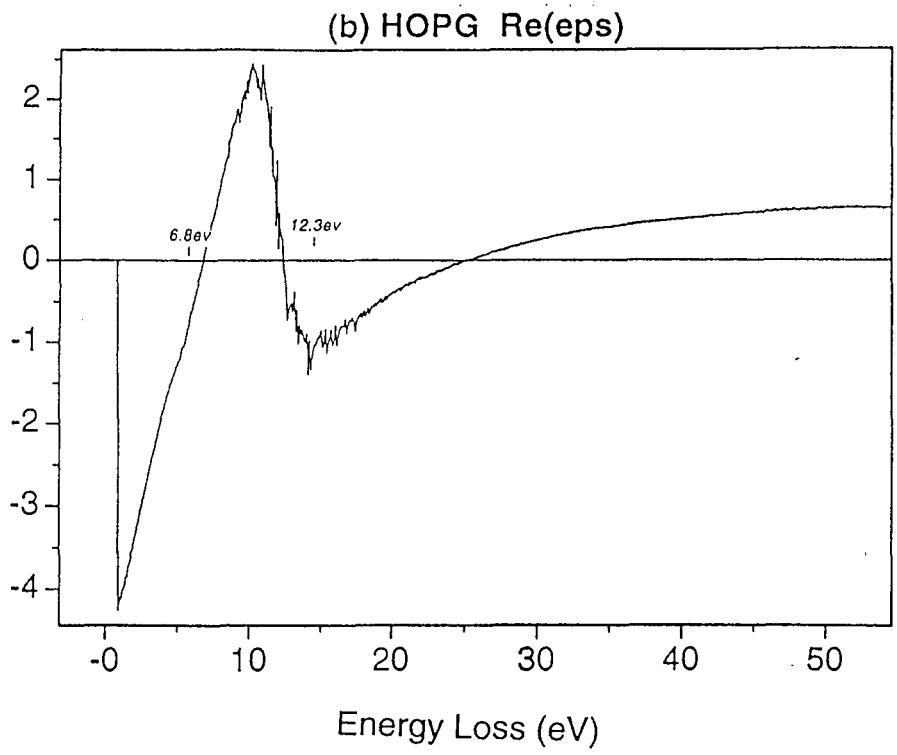
(b) HOPG Re(eps)
2
1
0
-1
-2
-3
-4
6.8ev
12.3ev
-0
10
20
30
40
50
Energy Loss (eV)

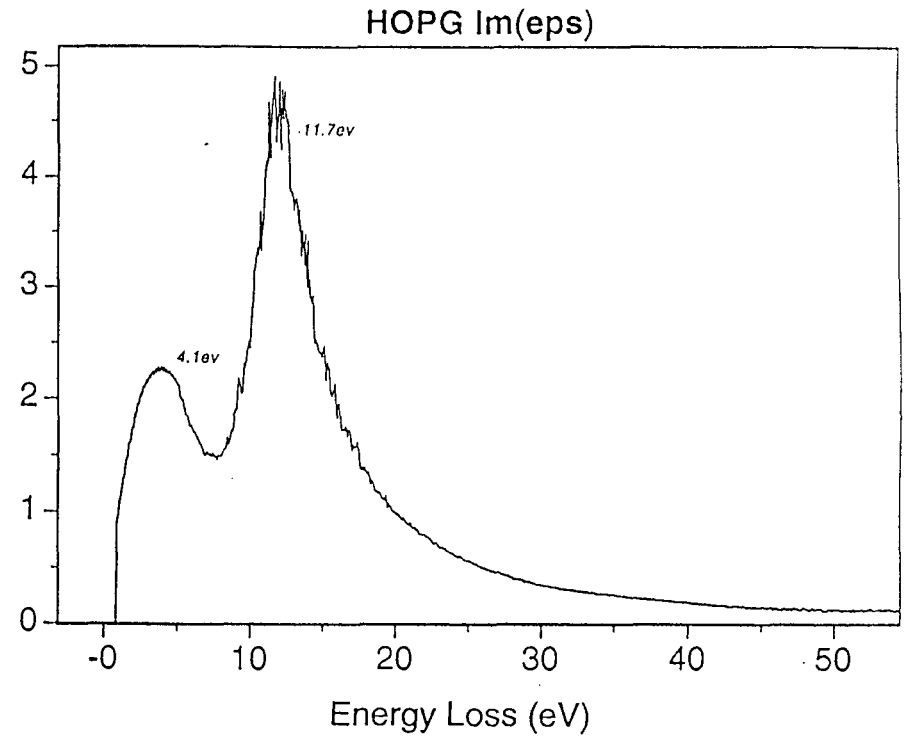
HOPG Im(eps)
5
4
3
2
1
0
11.7ev
4.1ev
-0
10
20
30
40
50
Energy Loss (eV)

(b)

**FIG. 3**

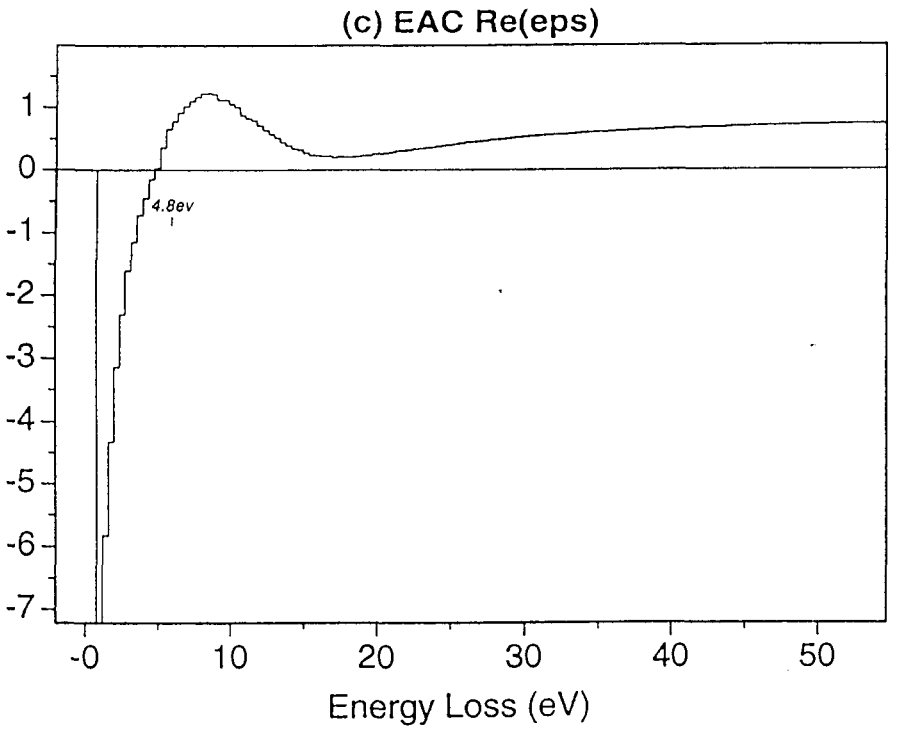
(c) EAC Re(eps)
1
0
-1
-2
-3
-4
-5
-6
-7
4.8ev
-0
10
20
30
40
50
Energy Loss (eV)

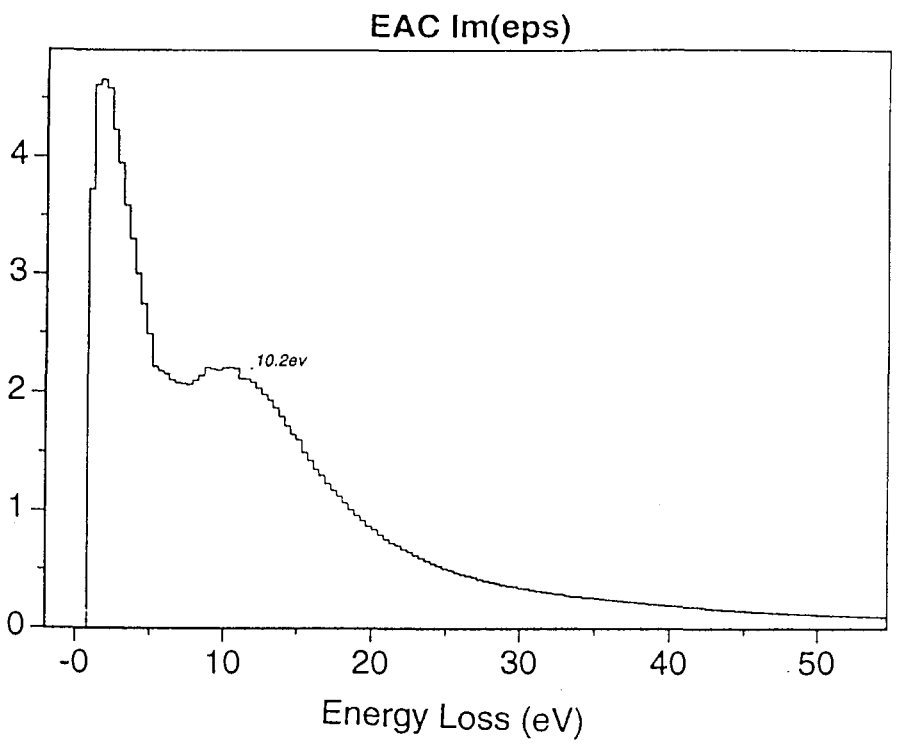
EAC Im(eps)
4
3
2
1
0
10.2ev
-0
10
20
30
40
50
Energy Loss (eV)

(c)

**FIG. 3**

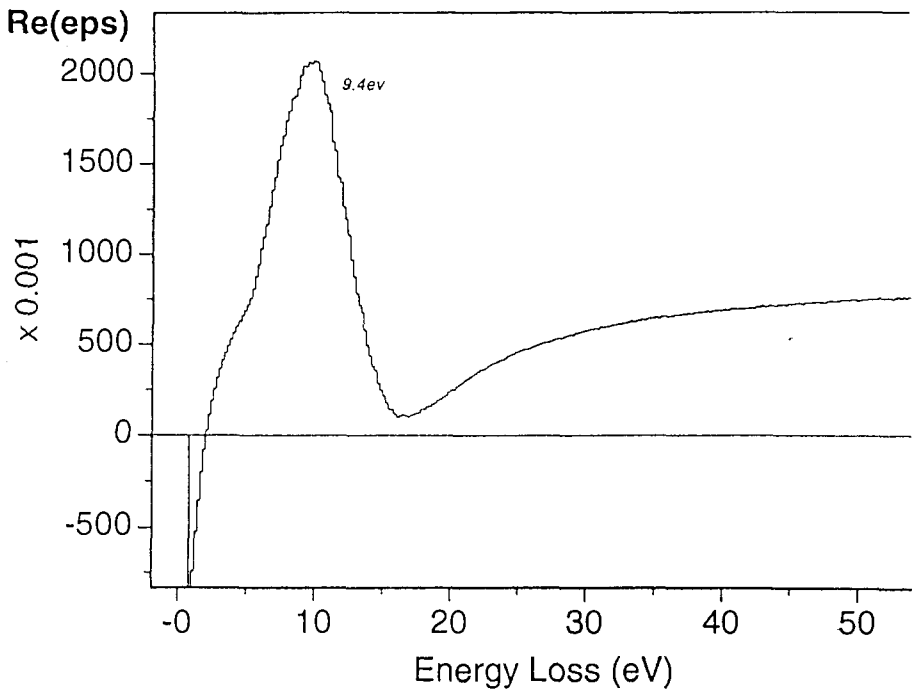
Re(eps)
2000
1500
1000
500
0
-500
x 0.001
9.4ev
-0
10
20
30
40
50
Energy Loss (eV)

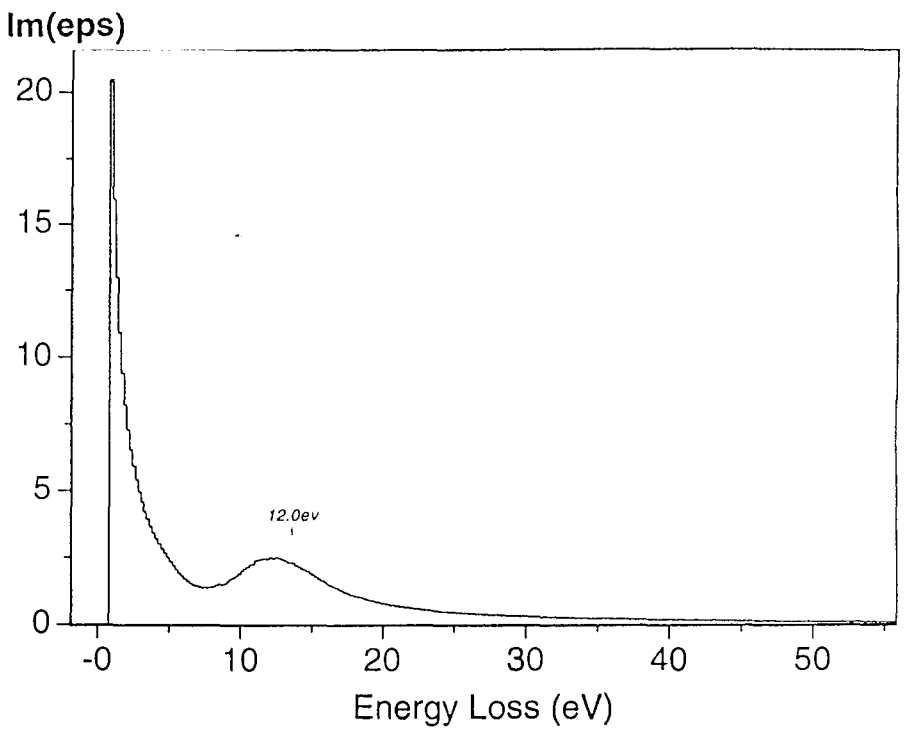
Im(eps)
20
15
10
5
0
12.0ev
-0
10
20
30
40
50
Energy Loss (eV)

(d)

**FIG. 3**